LA-UR- 99-268

Approved for public release; distribution is unlimited.

CONF-990110--

Title: ASPHERICAL BUBBLE DYNAMICS AND OSCILLATION TIMES

Author(s): Robert P. Godwin,* Edward J. Chapyak,* Joachim Noack,# and Alfred Vogel#

*Group XNH, Applied Theoretical and Computational Physics Division, Los Alamos National Laboratory, Los Alamos, NM 87545

#Medizinisches Laserzentrum Luebeck, 23562 Luebeck, Germany

Submitted to: Proceedings of Laser-Tissue Interaction X, Part of SPIE's International Symposium, BiOS'99, 23-29 January 1999, San Jose, CA (SPIE#3601A-67)

Los Alamos
NATIONAL LABORATORY

DISCLAIMER

Aspherical bubble dynamics and oscillation times

Robert P. Godwin [a], Edward J. Chapyak [a], Joachim Noack [b], and Alfred Vogel [b]

[a] Los Alamos National Laboratory, MS F664, Los Alamos, NM 87545, USA

[b] Medizinisches Laserzentrum Lübeck, D-23562 Lübeck, FRG

ABSTRACT

Novel features of aspherical bubble dynamics are explored. Time-resolved experimental photographs and simulations of large aspect ratio (length:diameter ~20) cylindrical bubble dynamics are presented. The experiments and calculations exhibit similar dynamics. A small high-pressure cylindrical bubble initially expands radially with hardly any axial motion. Then, after reaching its maximum volume, a cylindrical bubble collapses along its long axis with relatively little radial motion. The growth-collapse period of these very aspherical bubbles differs only slightly from twice the Rayleigh collapse time for a spherical bubble with an equivalent maximum volume. This fact justifies using the temporal interval between the acoustic signals emitted upon bubble creation and collapse to estimate the maximum bubble volume. As a result, hydrophone measurements can provide an estimate of the bubble energy even for aspherical bubbles. The prolongation of the oscillation period of bubbles near solid boundaries relative to that of isolated spherical bubbles is also discussed.

Keywords: aspherical dynamics, bubble dynamics, bubble energy, bubble oscillation period, cavitation, cylindrical dynamics, hydrodynamics, laser-medical applications, numerical methods

1. INTRODUCTION

The cavitation bubbles common in laser medicine are rarely perfectly spherical and are often located near tissue boundaries, in vessels, etc., which introduce aspherical dynamics. It is, on the other hand, desirable to be able to determine a bubble's volume and energy by very simple means. The bubble oscillation period can be determined from hydrophone measurements of the pressure pulses emitted at bubble generation and collapse. For spherical bubbles, the relation between bubble volume (radius) and oscillation period can often be approximated by the Rayleigh equation.[1,2] Bubbles associated with medical applications of lasers often have cylindrical geometry. Examples include long-pulse infrared laser experiments[3,4] and short-pulse water breakdown experiments.[5] We have checked the accuracy of the Rayleigh relation for aspherical dynamics by experimental and numerical investigations of cylindrical bubble dynamics in an infinite fluid volume and of initially spherical bubbles near a wall and in a tube. For isolated cylindrical bubbles, we found that the Rayleigh model is a surprisingly good approximation. On the other hand, our studies indicate nearby planar and tubular walls significantly increase the bubble oscillation period over that of Rayleigh's model. Nevertheless, if information on the location of the bubble with respect to a nearby wall is available, corrections to the Rayleigh collapse time allow an estimate of the bubble energy scale from hydrophone signals even in this case.

For a spherical cavitation bubble, Rayleigh's model gives a collapse time[6]

$$T_C = 0.915 R_o \sqrt{\frac{\rho}{p_\infty - p_v}}, \qquad (1)$$

when $p_v << p_\infty$; ρ, p_∞, p_v, and R_o are the fluid density, background fluid pressure, effective pressure of vapor and gas within the bubble which is assumed constant, and maximum radius of the bubble respectively. The bubble energy scale is

$$E_B = V_o (p_\infty - p_v), \qquad (2)$$

where V_o is the maximum bubble volume. The time difference between the acoustic wave emitted at bubble creation and the wave emitted upon collapse is $2T_C$. Thus, for a spherical bubble, a hydrophone measurement of the interval between the acoustic signals associated with bubble creation and collapse provides a convenient measure of the bubble radius, volume, and energy.

In Secs. 2. and 3., we describe experimental and numerical studies of aspherical bubble dynamics at the Medizinisches Laserzentrum Lübeck (MLL) and Los Alamos National Laboratory (LANL), respectively. The implications of our studies are discussed in Sec. 4. Our main conclusion is that experiments and simulations both demonstrate that, if an equivalent spherical radius is appropriately defined, Eq. (1) is a good approximation even for large aspect ratio cylindrical bubbles.

In addition, by using a correction procedure, Eq. (1) can be used for bubbles near solid planar walls. The reasons underlying the interesting dynamics of cylindrical bubbles are discussed in appendices.

2. EXPERIMENTS

2.1. Cylindrical bubbles

In photodisruption with ultrashort laser pulses, the breakdown region is elongated by self-focusing effects, and the bubbles produced by the expansion of the plasma generated during breakdown have a conical or even cylindrical shape.[5,7] In order to check whether Eq. (1) may be used to obtain the bubble volume of cylindrical bubbles by measuring their oscillation period, we created bubbles with a large aspect ratio and recorded their dynamics by high-speed photography.

The bubbles were generated by focusing Nd:YAG laser pulses (λ = 1064 nm) with 30 ps duration and up to 4 mJ pulse energy into a cuvette filled with distilled water. To minimize spherical aberrations, an ophthalmic contact lens was built into the cuvette wall.[8] We used a focusing angle of 4° and large pulse energies to produce strongly elongated plasmas and, hence, cylindrical bubbles. The bubbles were imaged with 2x magnification on the photocathode of an image converter camera (Hadland Photonics, Imacon 792, equipped with a Nikon 105/2.8 macro lens), and the bubble oscillations were recorded with a framing rate of 200,000 s^{-1}. The bubble volume was determined for each frame assuming rotational symmetry of the bubbles around the optical axis of the laser beam.[9]

Figure 1 presents a photographic series of the bubble dynamics at laser pulse energies of 1 mJ and 4 mJ. The bubbles have a strongly aspherical shape during most of their life cycle. Initially they expand radially with hardly any axial motion. Then, after reaching their maximum volume, they collapse along their long axis with relatively slow radial motion. Figure 2 shows the temporal evolution of the bubble length and diameter for the photo series of Fig. 1b. Both the length and diameter are, in different degrees, asymmetric for the expansion and collapse phases of the cylindrical bubble. The temporal evolution of the bubble volume, however, is more symmetric. This symmetry is demonstrated by plotting the equivalent diameter of a spherical bubble which has at each time the same volume as the cylindrical bubble investigated experimentally. In Fig. 3, the evolution of the equivalent spherical diameter of the cylindrical bubble of Fig. 1b is compared to the diameter-time curve of a spherical bubble with the same oscillation time. The curve for the spherical bubble is almost perfectly symmetric, whereas the curve for the cylindrical bubble is slightly asymmetric. The cylindrical bubble initially grows faster (due to the larger surface area of the initiating plasma), reaches its maximum size slightly before half of the collapse time has passed, and collapses somewhat more slowly than the spherical bubble. The maximum size of both bubbles is, however, almost the same.

The oscillation period of the very asymmetrical bubble of Fig. 1b (length to diameter ratio ~20:1 initially and 5:1 for the expanded bubble) only differed by 1.2% from twice the Rayleigh collapse time for a spherical bubble with an equivalent maximum volume. The oscillation time thus depends almost exclusively on the bubble volume and hardly at all on the bubble shape. This remarkable result justifies the use of Eq. (1) to estimate the maximum bubble volume of aspherical bubbles from the time interval between the acoustic signals emitted upon bubble creation and collapse. We will see in Sec. 2.2, however, that this applies for bubbles produced in the bulk of a liquid, but not for bubbles near material boundaries.

The fact that bubble wall segments with large curvature collapse rapidly and segments with small curvature collapse slowly leads to an invagination of the bubble ends at the long axis of the cylindrical bubble and thus bears a possibility for jet formation. This behavior becomes obvious in Fig. 1a where, after about 50 µs, a flattening of the bubble ends is observed. This flattening indicates that the ends have become concave and are beginning to jet inward. The tip of the jet is mostly obscured in the photographs and is only faintly visible after 55 µs and again during rebound after collapse at 65 µs. A similar feature was noted previously in bubble collapse near a solid boundary. Jet formation occurs very early when the bubble is elongated with the long axis perpendicular to the boundary.[11,12]

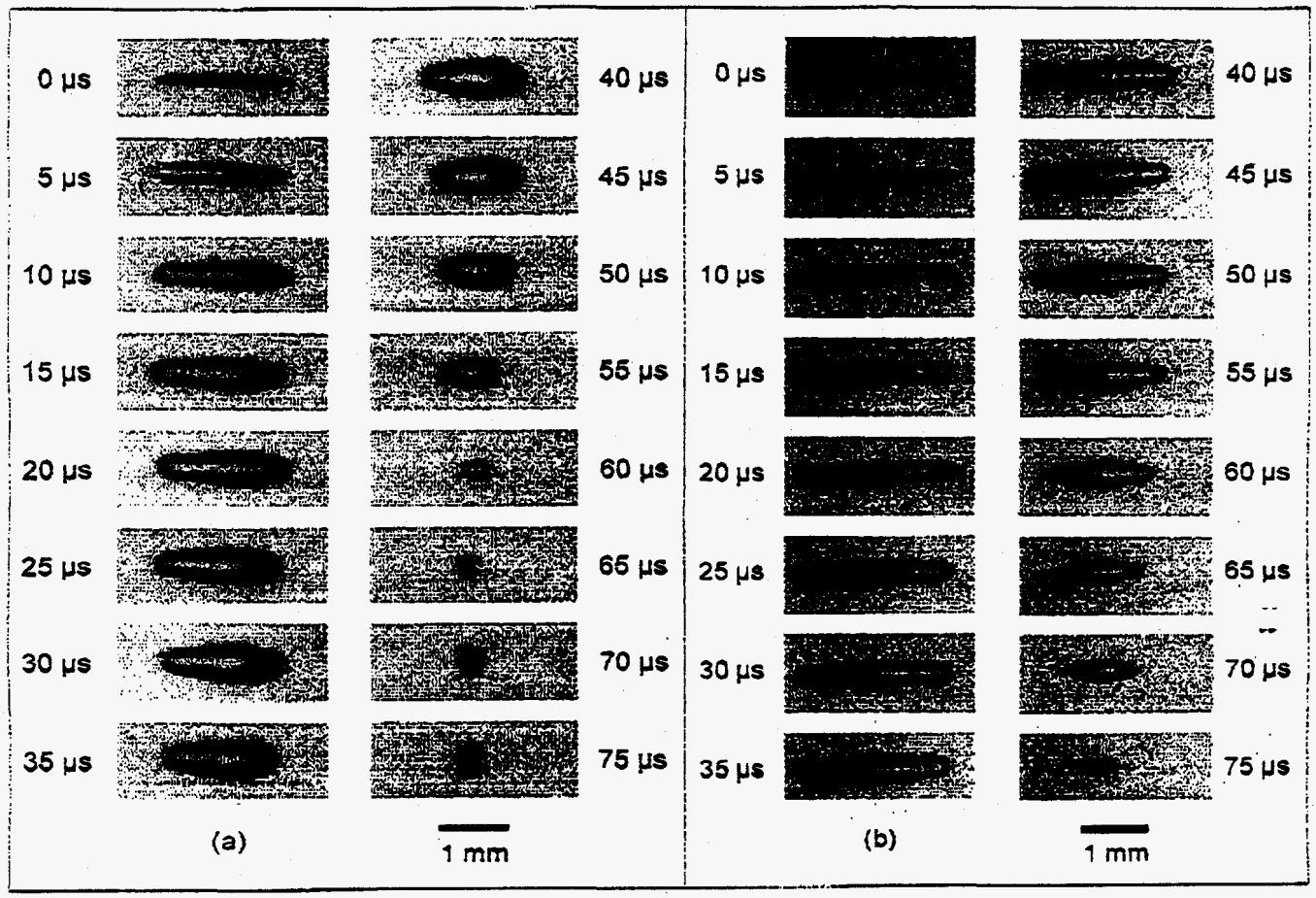

Fig. 1. Cylindrical bubble dynamics induced by 30-ps Nd:YAG laser pulses of a) 1 mJ and b) 4 mJ pulse energy which were focused into distilled water with a focusing angle of 4°. The laser light was incident from the left.

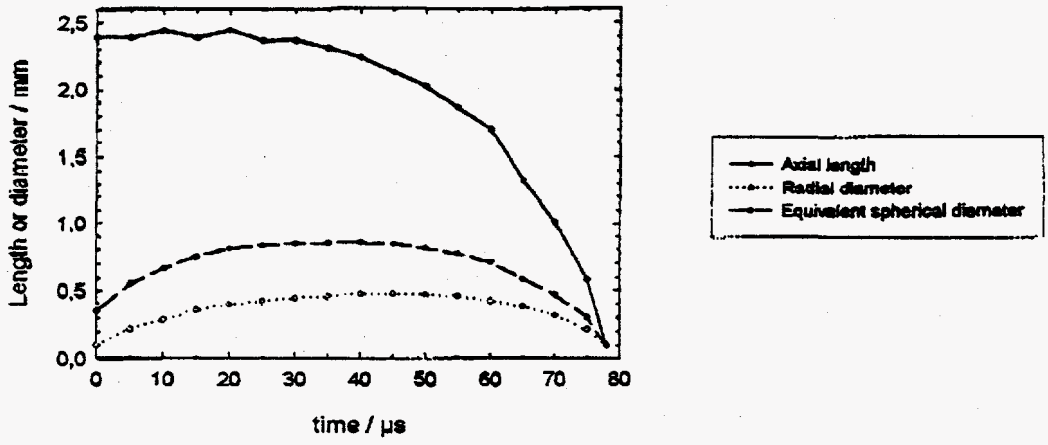

Fig. 2. Axial length and radial diameter as a function of time for the cylindrical bubble photo series of Fig. 1b. Also plotted is the diameter of a spherical bubble which has at each time the same volume as the cylindrical bubble.

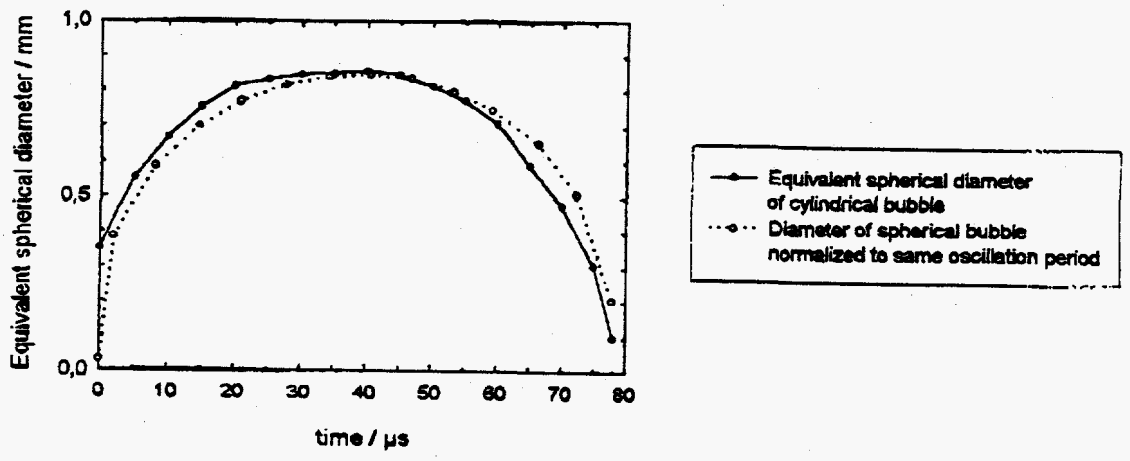

Fig. 3. Equivalent spherical diameter of the cylindrical bubble in Fig. 1b and diameter-time curve for a spherical bubble (data taken from Ref. 10). To facilitate comparison, the measurement data for the spherical bubble are normalized, using Eq. (1), to exhibit the same collapse time as the cylindrical bubble.

2.2. Bubbles near solid boundaries

When a cavitation bubble is produced in the vicinity of a solid boundary, its collapse time is prolonged as compared to the collapse of an isolated spherical bubble.[13,14,15] The prolongation factor k depends on the dimensionless distance

$$\gamma = s / R_{max} \tag{3}$$

between bubble and boundary, where s is the distance between bubble center and boundary at the time of bubble generation, and R_{max} is the maximum bubble radius. Rattray[14] derived an approximate relationship between the prolonged collapse T_C' and γ

$$\frac{T_C'}{T_C} = k = 1 + 0.41\frac{1}{2\gamma}, \tag{4}$$

where T_C is the collapse time of an isolated spherical bubble. In a previous publication,[15] we showed that Eq. (4) yields satisfactory results for $\gamma \geq 1$. It can, however, not be correct for very small γ, because it predicts $k \to \infty$ for $\gamma \to 0$.

In order to determine the prolongation factor k with better precision than in Refs. 14 and 15, we measured the bubble oscillation periods for laser-produced bubbles as a function of γ in a setup similar to that used in the experiments described in Sec. 2.1.[8] The bubbles were produced by Nd:YAG laser pulses with 6 ns duration and 5 mJ energy which were focused into a cuvette of distilled water with a convergence angle of 22°. The large focusing angle was chosen to produce highly spherical bubbles. The pulse-to-pulse fluctuations of the energy were ±2% and we assumed that, regardless of γ, the volume fluctuations of the laser-generated bubbles also remained within these limits. To avoid vignetting of the laser beam at the solid boundary, which would change the effective laser pulse energy, we focused the laser pulses through a glass plate (microscope slide) submerged into the cuvette. The glass plate served as the solid boundary (Fig. 4). The bubble oscillation periods $2T_C'$ at various γ values were determined using a PVDF hydrophone (CERAM miniature hydrophone) to detect the pressure pulses emitted upon bubble generation and collapse. The reference time $2T_C$ for spherical bubble oscillations was determined at $\gamma > 20$.

Figure 5 shows the results of our measurements compared to the predictions of Eq. (4). The agreement is fairly good for $\gamma \geq 1$, but for $\gamma < 1$, the actual collapse times (or k- values, respectively) are much smaller than predicted. Note that the collapse time has a maximum at $\gamma \approx 1$ and decreases for $\gamma \to 0$. This behavior is probably related to the fact that the collapse at $\gamma = 0$ is nearly hemispherical, that is, exhibits less deviation from spherical than the collapse at $\gamma \approx 1$. (In truly inviscid flow, there is no viscous boundary layer and the collapse of a hemispherical bubble on a wall is identical to the collapse of an isolated spherical bubble.)

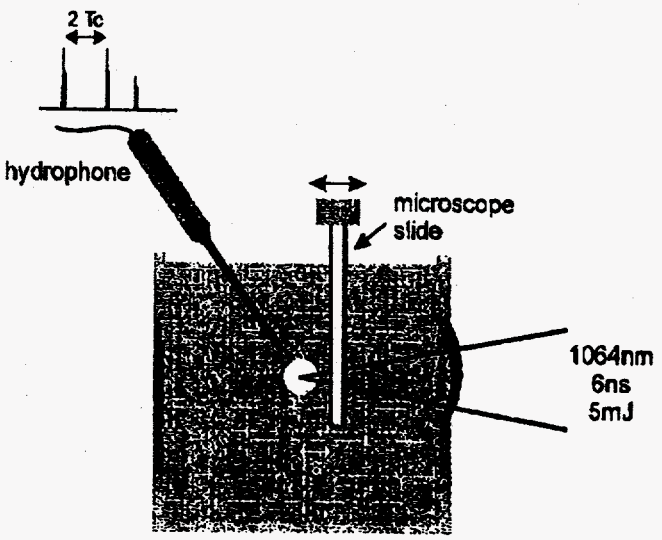

Fig. 4. Schematic of the experimental setup used for the investigation of bubble oscillation times near a solid wall.

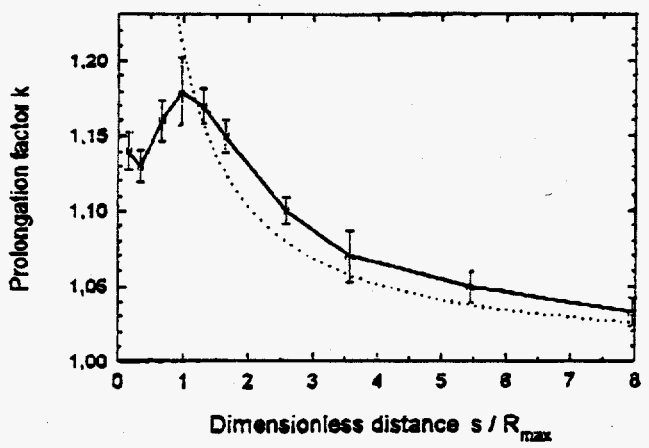

Fig. 5. Prolongation factor, k, for the oscillation period of a bubble near a solid wall plotted against the distance to the wall normalized by the maximum bubble radius. The dashed line represents the predictions of Eq. (4).

3. SIMULATIONS

3.1. Cylindrical bubbles

Using the LANL MESA2D code, we have numerically investigated the dynamics of cylindrical bubbles geometrically similar to those of the MLL experiments described in Sec. 2.1. The initial shape of the volume in the simulations was a cylinder with hemispherical end caps. Two initial conditions were examined: a water cavity filled with a χ=1.4 perfect gas at a pressure of either 50.5 or 505 bars; χ is the gas specific heat ratio. We compared the dynamics of these initially cylindrical bubbles (initial length to diameter ratio ~20:1) to the dynamics of spherical bubbles of the same initial volume and gas fill. Except for the cylindrical cavity shape, these numerical studies were similar to those we carried out earlier with a small high-pressure spherical seed bubble.[16,17,18] Our studies concentrated on the purely hydrodynamic aspects of asymmetrical bubble dynamics. In order to focus on hydrodynamics, we have chosen to avoid the potentially important issue of geometrical effects on the balance between vaporization and condensation of water vapor within the cavity by using an ideal gas equation of state for the bubble fill. In doing so, we have given up realistic energy accounting since the latent heat of water is large. By using a proper water equation of state, our computational tools can realistically model a water vapor filled bubble.[19] The symmetrizing effect of surface tension is a dominant feature of bubble dynamics for extremely small bubbles, for example, those produced upon explosive vaporization of melanosomes by laser pulses. Surface tension is, however, negligible for bubbles the size of those in the experiments described in Sec. 2, and it is not modeled in the simulations discussed here.

Figure 6 shows the MESA simulated evolution of bubble shape for the low (50.5 bar) initial pressure case. The bubble retains a cylindrical shape throughout most of the dynamics, but finally collapses with jet formation inward along the cylindrical axis. The behavior in this simulation is similar to that of the experimental photo series of Fig. 1b. The axial jetting, which is easy to see in the collapse phase of the simulation, is present (but difficult to see) in experimental photos.

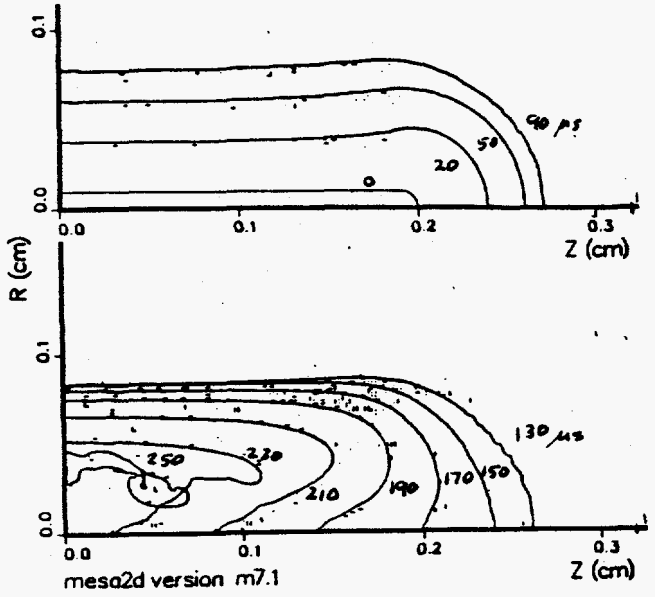

Fig. 6. Simulated dynamics of a cylindrical water bubble with an initial length:diameter ratio of 20 and an initial ideal gas fill pressure of 50.5 bar = 5.05 MPa; a) upper plot -- expansion phase and b) lower plot -- contraction phase.

In Fig. 7, the evolution of bubble shape calculated for the cylindrical bubble with an initial fill pressure of 505 bars is displayed. This bubble grows to a more spherical shape (aspect ratio 1.2:1 at maximum expansion) before collapsing with an inward jet developing along the cylindrical axis. With still higher initial pressures, the bubble dynamics becomes nearly spherical at all but very early and very late times in the growth-collapse cycle.

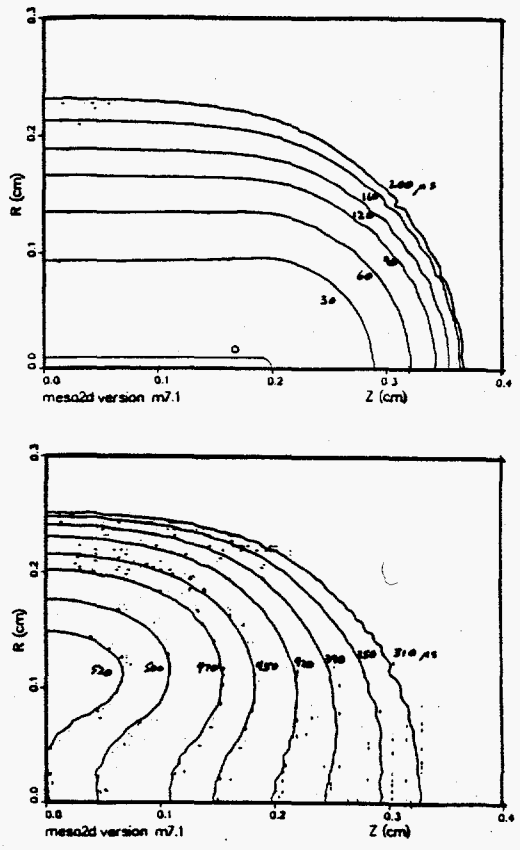

Fig. 7. Simulated dynamics of a cylindrical bubble with an initial length:diameter ratio of 20 and an initial ideal gas fill pressure of 505 bar = 50.55 MPa; a) upper plot -- expansion and b) lower plot -- contraction.

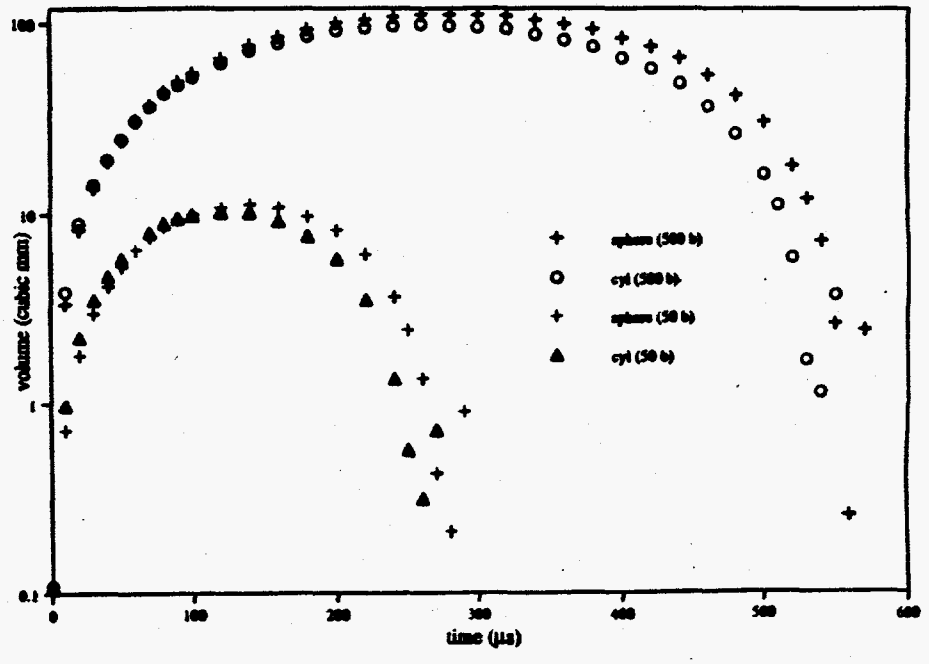

Fig. 8. Plot of volume vs. time for paired spherical and cylindrical simulations. The initial volume was identical in the four cases shown, but one pair was run with 50.5 bar initial pressure and the second with 505 bar initial pressure. The cylindrical cases are those of Figs. 6 and 7.

We have plotted in Fig. 8 the volume as a function of time for the four cases simulated. Of greatest interest is the fact that, as in the MLL experiments of Sec. 2.1, the collapse times are quite similar between the cylindrical and spherical cases. Initially the cylindrical bubbles, having more surface area than the spherical bubbles of the same volume, increase their volume faster than do the spherical bubbles. This situation occurs because the local pressure gradients, and therefore the local velocities, must be similar in both cases. When the bubble reaches its maximum volume, the water surrounding the bubble is quiescent in the spherical case. At the maximum spherical volume, all of the kinetic energy has been converted to potential energy. In the case of a cylindrical bubble, the bubble is still growing radially after it has begun to contract axially. In the cylindrical case, the kinetic energy invested in the fluid is never completely converted to bubble potential energy because of the lack of quiescence at the maximum volume. As a result, the maximum bubble volume for a given initial seed bubble energy is somewhat larger for a spherical bubble than for a cylindrical bubble. This minor difference in the partition of energy makes the growth-collapse oscillation time of a cylindrical bubble less than that of a spherical bubble of equivalent initial energy, but only slightly less. As in the experiment (Fig. 3), the cylindrical bubble reaches its maximum slightly before half of the oscillation cycle has passed.

3.2. Bubbles near solid boundaries

The MLL experimental results of Sec. 2.2 can be compared for specific γ values to data from numerical investigations on bubble dynamics. Szymczak et al.[20] calculated the dynamics for $\gamma=1$ and were able to follow the dynamics after the jet hit the opposite bubble wall. In this way, they could determine when the minimum bubble volume was reached and the collapse pressure transient emitted. The calculations yielded a prolongation factor k=1.20, in good agreement with the experimental result, $k = 1.18\pm0.02$.

We simulated with MESA2D bubble dynamics near a rigid wall for $\gamma=1.1$ with three slightly different situations:[21]

1. Collapse of an initially spherical empty cavity of radius 1 mm (that is, a problem corresponding to Rayleigh void collapse except near a wall),
2. a 1mm radius spherical cavity with a low-pressure gas fill, and
3. the growth-collapse cycle of a small high-pressure (505 bar) spherical seed bubble with the pressure chosen so that, in the absence of acoustic emission, the maximum volume would correspond to that of the bubble of case 2 in the absence of a wall. The k values deduced from these three numerical simulations are 1.18, 1.19, and 1.16, respectively; all in good agreement with both the MLL measurements and the simulation of Szymczak et al.

We have also simulated the effect of both elastic and rigid tubular walls on the bubble oscillation period of an initially high-pressure seed bubble.[22] These cases approximate the configuration of many laboratory and clinical laser medical applications. As one might expect, the period prolongation of nearby tubular walls is much stronger than that of a nearby planar wall. For comparable bubble-wall distances, a planar wall produces a prolongation of ≤20% and a tubular wall a prolongation of ~2x.

Knowledge of the prolongation factor $k(\gamma)$ (Fig. 5) and of the stand-off distance s between the initial bubble center and a planar solid boundary allows the determination of the cavitation bubble size R_{max} by measuring the oscillation period $2T'_C$ with a hydrophone. In a first step, approximate values R_{max1} and γ_1 are calculated from the experimental data using Eq. (1). Correction of $2T'_C$ by the factor $k_1(\gamma_1)$ yields the more precise values R_{max2} and γ_2; correction of $2T'_C$ by the factor $k_2(\gamma_2)$ yields R_{max3}, and so on, until the required precision is reached.

4. SUMMARY

Both experiments and simulations show convincingly that the oscillation period of large aspect ratio cylindrical bubbles differs only slightly from twice the Rayleigh collapse time for a spherical bubble with an equivalent maximum volume. (We have not rigorously proved that one cannot imagine extremely long cylindrical bubbles for which this is not true. We are convinced, however, that it is true for bubbles of interest in laser medical applications.) The oscillation time depends almost exclusively on the bubble volume and hardly at all on the bubble shape. This remarkable result justifies the use of Eq. (1) to estimate the maximum bubble volume of aspherical bubbles from the time interval between the acoustic signals emitted upon bubble creation and collapse. In order to use Eq. (1), one needs only to define the equivalent maximum bubble radius as

$$R_o \equiv \left(\frac{3}{4\pi}V_o\right)^{1/3}, \qquad (5)$$

where V_o is the maximum bubble volume. The bubble energy of large aspect ratio cylindrical bubbles can be estimated using Eq. (2). This approximation will be also be useful for non-spherical bubbles with shapes other than cylindrical. Miles showed that Eq. (1) can be applied to the collapse of cavities of arbitrary shape.[6]

This approximation cannot, however, be used with bubbles near material interfaces. Experimental, analytical, and numerical investigations show that nearby rigid walls significantly increase the bubble growth-collapse period. This prolongation of the period is a systematic function of the distance of the bubble from the wall. As a result, if one knows the distance of a bubble from a nearby wall and the prolongation factor $k(\gamma)$, one can relate the measured growth-collapse oscillation period determined from hydrophone signals to the maximum bubble volume and thereby to the bubble energy.

Bubble dynamics close to a solid boundary exhibits larger deviations from twice the Rayleigh collapse time than does the dynamics of large aspect ratio cylindrical bubbles. This result is, at first sight, surprising since the deviations of the bubble shape from spherical for a bubble near a wall are less obvious than in the case of isolated cylindrical bubbles. Closer investigation reveals, however, that bubble collapse at a material boundary is accompanied by the development of toroidal flow (ring vortex)[11] which distorts and delays flow toward the bubble center. A similar distortion is not observed in cylindrical bubble collapse. A second reason for the delayed collapse of a bubble close to a wall is that the wall inhibits fluid flow toward the bubble. The flow around an isolated cylindrical bubble is, in contrast, governed only by the difference between the hydrostatic pressure and the pressure within the bubble and by inertial forces.

The investigations in this paper focused on bubbles generated by laser pulses considerably shorter than the bubble oscillation time. The bubble dynamics is modified when free-running laser pulses with a duration comparable to the bubble oscillation time are used.

For fiber delivery, the accuracy of Eq. (1) was confirmed when Q-switched holmium laser pulses were used for bubble generation.[3] When Er:YSGG pulses were used, the oscillation times were, however, shorter than the collapse time predicted by Eq. (1).[3] This phenomenon is not yet completely explained and may be associated with violation of the conditions for which Eq. (1) is valid.[6]

Further aspects of cylindrical bubble dynamics are discussed in the appendices. In Appendix A, we demonstrate that one cannot create in cylindrical geometry a radial collapse model analogous to the spherical Rayleigh model. In Appendix B, we discuss the curious fact that cylindrical bubbles move ever closer to spherical.

ACKNOWLEDGMENTS

The efforts of R. P. G. and E. J. C. were supported by a Cooperative Research and Development Agreement (CRADA) between Los Alamos National Laboratory (Department of Energy), Oregon Medical Laser Center, and Palomar Medical Technologies. J. N. and A. V. were supported by the Deutschen Forschungsgemeinschaft and the US Air Force. R. P. G. thanks Kin Foong Chan, a University of Texas at Austin student, for questions which stimulated his interest in cylindrical dynamics.

APPENDICES

A. There is no cylindrical analog of Rayleigh cavity collapse

Rayleigh's cavity collapse model is extremely useful in bubble dynamics, but it cannot be naively applied to non-spherical bubbles. While it may seem intuitively obvious that a similar model can be used for cylindrical bubbles of "large enough" length to diameter ratio, one cannot create a cylindrical analog of the spherical Rayleigh paradigm. Following the development of the Rayleigh model demonstrates the impossibility of a cylindrical analog. For the spherical case, the velocity of flow and its associated velocity potential are,[1,2]

$$v_r = -\partial\phi/\partial r = -R^2\dot{R}/r^2 \qquad \text{and} \qquad \phi = -R^2\dot{R}/r, \tag{A.1}$$

where R and $\dot{R}$ are the cavity wall location and velocity. The cylindrical analogs are

$$v_r = -\partial\phi/\partial r = -R\dot{R}/r \qquad \text{and} \qquad \phi = -R\dot{R}\ln r. \tag{A.2}$$

The required boundary conditions cannot be satisfied in cylindrical geometry because the potential does not vanish at infinity. This mathematically rigorous proof of the impossibility of a cylindrical model has profound implications for the dynamics of cylindrical bubbles.

Using insight gained from Eqs. (A.1) and (A.2), together with the experiments and simulations of Secs. 2.1 and 3.1, we postulate that the radial portion of the dynamics of a large aspect ratio cylindrical bubble will behave as if

$$v_r = -\partial\phi/\partial r = -R^{1+\alpha}\dot{R}/r^{1+\alpha} \qquad \text{and} \qquad \phi = -R^{1+\alpha}\dot{R}/r^{\alpha}. \tag{A.3}$$

This postulated potential leads to the "generalized Rayleigh" cavity wall equation of motion

$$R\ddot{R} + \frac{(2+\alpha)}{2}\dot{R}^2 + \alpha\frac{P_\infty}{\rho} = 0 \tag{A.4}$$

with the solution

$$\dot{R}^2 = \left(\frac{2\alpha}{2+\alpha}\right)\frac{P_\infty}{\rho}\left[\left(\frac{R_o}{R}\right)^{2+\alpha} - 1\right]. \tag{A.5}$$

When α=1, Eqs. (A.4) and (A.5) reduce to the familiar spherical Rayleigh case. A zero radial velocity is predicted for α=0, pure cylindical geometry. This result is interesting since we found in our investigations a very small initial collapse velocity for large aspect ratio cylindrical bubbles; α is related to the aspect ratio of a cylindrical bubble of finite length and is time dependent.

In the *spherical* case, significant fluid dynamics extends over a volume several times that of the bubble. During cavity collapse, the bubble potential energy is transformed into fluid kinetic energy

$$\Delta PE = P_\infty(V_o - V) = \Delta KE = \tfrac{1}{2}m_e v_e^2. \tag{A.6}$$

Given appropriate definitions for the effective mass, m_e, and velocity, v_e, Eq. (A.6) provides an accurate description of the collapse dynamics. Let $v_e = \dot{R}$ and assume the fluid mass $m_e = \rho 4\pi R^2 \Delta R$, where ΔR is the fluid thickness just outside the bubble, to obtain

$$\dot{R}^2 = \left(\frac{2}{3}\right)\frac{P_\infty}{\rho}\left[\left(\frac{R_o}{R}\right)^3 - 1\right]\frac{R}{\Delta R}. \tag{A.7}$$

Comparison with the the proper solution of the spherical Rayleigh model, that is, Eq. (A.5) with α=1, shows $\Delta R = R$. This result justifies the definition of the Minnaert effective mass, $m_e = \rho 4\pi R^3$, as three times the missing cavity mass and demonstrates that the important dynamics associated with a spherical bubble occurs near the bubble. Applying the same heuristic approach to the *cylindrical* case yields a distinctly different result. One finds the collapse velocity equation

$$\dot{R}^2 = \frac{P_\infty}{\rho}\left[\left(\frac{R_o}{R}\right)^2 - 1\right]\frac{R}{\Delta R}. \tag{A.8}$$

In order for this result to agree with Eq. (A.5),

$$\Delta R = \left(\frac{2+\alpha}{2\alpha}\right)R. \tag{A.9}$$

In cylindrical geometry with α=0, the predicted radial region of bubble influence extends to infinity.

Consider a large aspect ratio cylindrical bubble of radius R and half-length Z. Viewed from a sufficiently great distance, the bubble will appear as a point with dynamics similar to those of a spherical cavity. For the sake of this discussion, assume that the fluid flow dynamics takes on a spherical character at a distance ~2Z from the bubble center. We expect that the flow dynamics will behave as if $\Delta R \sim 2Z$ (equivalently, $\alpha \sim R/(2Z)$) and Eqs. (A.5) and (A.8) predict

$$\dot{R}^2 \sim \frac{R}{2Z}\frac{P_\infty}{\rho}\left[\left(\frac{R_o}{R}\right)^2 - 1\right], \tag{A.10}$$

that is, low radial collapse velocities. The collapse dynamics occurs predominately in the regions of small radius of curvature at the ends of cylindrical bubbles. A large fluid mass must be accelerated for the bubble collapse normal to the bubble axis resulting in a small average radial fluid velocity. In contrast, the axial velocity can be very high at the bubble ends, because little mass is involved in this motion.

B. Cylindrical dynamics moves toward spherical

Consider a bubble with a surface figure described by the combination of a spherical surface and a P_2 surface harmonic. We assume an inviscid fluid and an ideal gas bubble fill. The bubble surface is

$$r_S(\theta,t) = R(t) + a_2(t)P_2(\mu), \tag{B.1}$$

where $\mu = \cos\theta$. Let ρ_- be the liquid density and p_∞ the pressure at infinity. The bubble contains a constant gas mass with a polytropic exponent χ. The equations of motion are the Rayleigh-Plesset equation[6]

$$R\ddot{R} + \frac{3}{2}\dot{R}^2 = v_o^2\left[\left(\frac{R_n}{R}\right)^{3\chi} - 1\right], \tag{B.2}$$

where R_n is the equilibrium radius and $v_o \equiv \sqrt{P_\infty/\rho}$, and

$$\ddot{a}_2 + 3\frac{\dot{R}}{R}\dot{a}_2 - \frac{\ddot{R}}{R}a_2 = 0. \tag{B.3}$$

Equation (B.3) is valid only for small amplitudes.[13,23] As a concrete example, we examine the initial bubble geometry $R(0) = R_o$ and $a_2(0) = A_o$, so that $r_S(\theta,0) = R_o + A_o P_2(\mu)$ or, equivalently,

$$Z = r_S(0,0) = R_o + A_o P_2(1) = R_o + A_o \tag{B.4a}$$

and

$$R = r_S(\pi/2,0) = R_o + A_o P_2(0) = R_o - A_o/2. \tag{B.4b}$$

The $\dot{R}$ term in Eq. (B.3) can be neglected during the early phase of collapse (and late phase of growth) giving

$$\ddot{a}_2/a_2 - \ddot{R}/R \approx 0; \tag{B.7}$$

$a_2 = kR$, with k constant, is a solution. Thus, $Z \approx R_o(1+k)$ and $R \approx R_o(1-k/2)$ for small times. The corresponding bubble length:diameter aspect ratio of this cylindrical bubble is then

$$\frac{Z}{R} \approx \frac{1+k}{1-k/2} = \frac{Z_o}{R_o}. \tag{B.8}$$

Near the bubble maximum its volume, but not its shape, changes with time. Figure 9 is a plot of the length to diameter ratio as a function of normalized time for the experimental photo series of Fig. 1b. The bubble aspect ratio is a weak function of time after the bubble expansion in qualitative agreement with Eqs. (B.7) and (B.8).

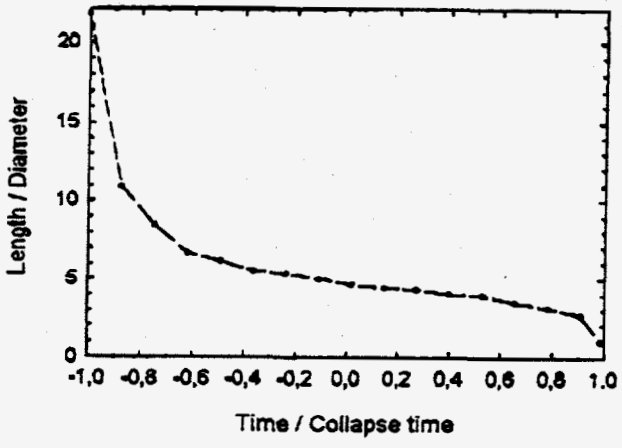

Fig. 9. Time evolution of the aspect ratio, length:diameter, for the experimental photo series of Fig.1b. The simulations of Figs. 6 and 7 have a similar aspect ratio history.

Later in the dynamics the velocity product term of Eq. (B.3) causes bubble shape changes. More importantly, time reversal changes the sign of the velocity product term, since $\dot{R}$ is an odd function and R an even function of t. By about 70% of the collapse time, τ_o, the magnitude of the normalized velocity/radius ratio, $\dot{R}\tau_o/R$, is above 2 and increasing rapidly with time causing a rapidly changing aspect ratio. As a result of the change of sign of the velocity term, a tiny high-pressure cylindrical bubble will expand rapidly in the radial direction. Near its maximum volume, it will expand and then contract rather slowly with little shape change. Finally, during the later stages of collapse, it will rapidly contract axially.

Figure 9 exhibits the dynamics history. The aspect ratios as a function of time for the MESA simulations of Figs. 6 and 7 are similar. During the entire dynamics history, the length/radius ratio of the cylindrical bubble constantly decreases, that is, the bubble dynamics brings the bubble ever nearer spherical. (Actually, inertial effects cause the dynamics to overshoot spherical. The axial collapse at late time drives the aspect ratio to less than unity producing inward jetting along the axis.)

REFERENCES

1. Lord Rayleigh, "On the pressure developed in a liquid during the collapse of a spherical cavity," *Phil. Mag.* **34**, pp. 94-98, 1917.
2. J. Lighthill, Sec. 7.2, "Spherically symmetrical motions," *An Informal Introduction to Theoretical Fluid Mechanics*, Clarendon Press, Oxford, 1986.
3. M. Frenz, H. Pratisto, F. Konz, E. D. Jansen, A. J. Welch, and H. P. Weber, "Comparison of the Effects of Absorption Coefficient and Pulse Duration of 2.12 μm and 2.79 μm Radiation on Laser Ablation of Tissue," *IEEE Jour. Quant. Elec.* **32** (12), pp. 2025 -2036, 1996.
4. K. F. Chan, T. J. Pfefer, D. X. Hammer, E. D. Jansen, M. Frenz, and A. J. Welch, "Fluorescence-Based Temperature Measurement in Laser-Induced Vapor Bubbles," *Laser Tissue Interaction IX, Proc. SPIE* **3254**, pp. 276-286, 1998.
5. A. Vogel, J. Noack, K. Nahen, D. Theisen, R. Birngruber, D. X. Hammer, G. D. Noojin, and B. A. Rockwell, "Laser-induced breakdown in the eye at pulse durations from 80 ns to 100 fs," *Applications of Ultrashort-Pulse Lasers in Medicine and Biology, Proc. SPIE* **3255**, pp. 34-49, 1998.
6. M. S. Plesset and A. Prosperetti, "Bubble Dynamics and Cavitation," *Ann. Rev. Fluid Mech.* **9**, pp. 145-185, 1977.
7. J. Noack, D. X. Hammer, G. D. Noojin, B. A. Rockwell, and A. Vogel "Influence of pulse duration on mechanical effects after laser-induced breakdown in water," *J. Appl. Phys.* **83**, pp. 7488-7495, 1998.
8. A. Vogel, K. Nahen, D. Theisen, and J. Noack "Plasma formation in water by picosecond and nanosecond Nd:YAG laser pulses - Part 1: Optical breakdown at threshold and superthreshold irradiance," *IEEE J. Selected Topics Quantum Electron.* **2**, pp. 847-860, 1996.
9. J. Noack, "Optischer Durchbruch in Wasser mit Laserpulsen zwischen 100 ns und 100 fs," *PhD Dissertation*, Medical University of Lübeck, Lübeck (Germany), 1998.
10. W. Lauterborn, "Kavitation durch Laserlicht", *Acustica* **31**, pp. 51-78, 1974.
11. A. Vogel, W. Lauterborn, and R. Timm, "Optical and acoustic investigations of the dynamics of laser-produced cavitation bubbles near a solid boundary," *J. Fluid Mech.* **206**, pp. 299-338, 1989.
12. A. Philipp and W. Lauterborn, "Cavitation erosion by single laser-produced bubbles," *J. Fluid Mech.* **361**, pp. 75-116, 1998.
13. R. H. Cole, Chap. 8, "Motion of the Gas Sphere," *Underwater Explosions*, Princeton U, Princeton, 1948.
14. M. Rattray, *PhD Dissertation*, California Institute of Technology, 1951; quoted in M. S. Plesset and 15.R. B. Chapman "Collapse of an initially spherical vapour cavity in the neighbourhood of a solid boundary," *J. Fluid Mech.* **47**(2), pp. 283-290, 1971.
15. A. Vogel and W. Lauterborn, "Acoustic transient generation by laser produced cavitation bubbles near solid boundaries", *J. Acoust. Soc. Am.* **84**, pp. 719-731, 1988.
16. E. J. Chapyak and R. P. Godwin, "Numerical Studies of Bubbles in Laser Thrombolysis," *Lasers in Surgery: Advanced Characterization, Therapeutics, and Systems VI, Proc. SPIE* **2671**, pp. 84-87, 1996.
17. E. J. Chapyak, R. P. Godwin, S. A. Prahl, and H. Shangguan, "A Comparison of Numerical Simulations and Laboratory Studies of Laser Thrombolysis," *Lasers in Surgery: Advanced Characterization, Therapeutics, and Systems VII, Proc. SPIE* **2970**, pp. 28-34, 1997.
18. E. J. Chapyak and R. P. Godwin, "Physical Mechanisms of Importance to Laser Thrombolysis," *Lasers in Surgery: Advanced Characterization, Therapeutics, and Systems VIII, Proc. SPIE* **3245**, pp. 12-18, 1998.
19. E. J. Chapyak, R. P. Godwin, and A. Vogel, "Comparison of Numerical Simulations and Laboratory Studies of Shock Waves and Cavitation Bubble Growth Produced by Optical Breakdown in Water," pp. 335-3432, 1997.
20. W. G. Szymczak, J, C. W. Rogers, J. M. Solomon, and A. E. Berger, "A numerical algorithm for hydrodynamic free boundary problems," *J. Comput. Phys.* **106**, pp. 319-336, 1993.
21. R. P. Godwin, E. J. Chapyak, S. A. Prahl, and H. Shangguan, "Laser Mass Ablation Efficiency Measurements Indicate Bubble-Driven Dynamics Dominates Laser Thrombolysis," *Lasers in Surgery: Advanced Characterization, Therapeutics, and Systems VIII, Proc. SPIE* **3245**, pp. 4-11, 1998. Also unpublished work.
22. E. J. Chapyak and R. P. Godwin, "Simulations of Laser Thrombolysis," *Lasers in Surgery: Advanced Characterization, Therapeutics, and Systems IX, Proc. SPIE* **3590**, 1999 (to be published).
23. H. W. Strube, "Numerische Untersuchungen zur Stabilität nichtsphärisch schwingender Blasen," *Acustica* **25**, pp. 289-303, 1971.